LETTER | APRIL 01 2025

On regionalization of thermochemical nonequilibrium in scramjet

Jingying Wang ; Shiyue Zhang; Jiaao Hao ; Wei Zhao ; Xinglian Yang; Chunhian Lee

Physics of Fluids 37, 041702 (2025)
https://doi.org/10.1063/5.0264195

Physics of Fluids LETTER pubs.aip.org/aip/pof

On regionalization of thermochemical nonequilibrium in scramjet

Cite as: Phys. Fluids **37**, 041702 (2025); doi: 10.1063/5.0264195
Submitted: 9 February 2025 · Accepted: 12 March 2025 ·
Published Online: 1 April 2025

Jingying Wang,[1,a)] Shiyue Zhang,[1] Jiaao Hao,[2] Wei Zhao,[1] Xinglian Yang,[1] and Chunhian Lee[1]

AFFILIATIONS

[1]School of Energy and Power Engineering, Shandong University, Jinan 250061, China
[2]Department of Aeronautical and Aviation Engineering, The Hong Kong Polytechnic University, Hong Kong 999077, China

[a)]Author to whom correspondence should be addressed: wjy_sdu@sdu.edu.cn

ABSTRACT

Thermochemical nonequilibrium significantly affects flow and combustion characteristics in the scramjet of air-breathing hypersonic vehicle. However, a clear map of thermochemical nonequilibrium in scramjets has not been reported. This work simulates thermochemical nonequilibrium combustion flows in Deutsches Zentrum für Luft-und Raumfahrt and HyShot II scramjets, respectively, and shows the comprehensive vibrational and chemical nonequilibrium regionalizations in both scramjets based on defined Damköhler numbers. Vibrational nonequilibrium is mainly located at the edge of the flame, while chemical nonequilibrium is mostly found inside the flame. As the observational length scale extends, the nonequilibrium zone remarkably spreads in the scramjet, which should be paid attention to in future research.

The air-breathing hypersonic vehicle is of great significance to national defense and civil aviation, with its core propulsion system being the scramjet.[1,2] For a flight Mach number over 8 (Ma > 8), that is the so-called high-Mach flight,[3,4] thermochemical nonequilibrium effects inside the scramjet should be paid special attention to. Recent studies have shown that thermochemical nonequilibrium effects significantly influence flow and combustion characteristics in some parts of the high-Mach scramjet. The compressions of forebody/inlet shock waves are responsible for the initialization of thermodynamically vibrational excitation in the scramjet.[3] The pseudoshock length in the scramjet isolator increases remarkably under the vibrational nonequilibrium with the shock wave structure moving upstream.[5] The vibrational nonequilibrium can delay the flame ignition in a supersonic coflow with the fuel jet,[6] while it can also counterintuitively lead to the much earlier ignition for a fuel jet injected into the supersonic crossflow than in the equilibrium flow.[7] Additionally, thermochemical nonequilibrium would induce the cooling effect in the expanding nozzle of the scramjet.[8] Although the forebody, inlet, isolator, combustor, and nozzle are different parts of the scramjet, they must be connected as a whole to realize the high-efficiency propulsion. Correspondingly, the thermochemical state in each scramjet part also should be considered integrally, which requires a clear zonal recognition of thermochemical nonequilibrium for a whole scramjet. However, to our knowledge, there has not been any published work to show it.

Thermochemical nonequilibrium in a flow can be recognized depending on the dimensionless Damköhler number (*Da*), defined as the ratio of flow residence timescale to thermodynamically vibrational relaxation timescale or chemical reaction timescale.[9] Generally, the thermodynamically vibrational relaxation timescale of molecular species is calculated using the Millikan–White relation,[10,11] which will be introduced in detail in the following content. However, how to compute timescales of flow residence and chemical reaction is still a matter of some uncertainty.

Flow residence time, τ_f, can be directly defined as the ratio of flow characteristic length (L) to the speed (U), that is, $\tau_f = L/U$. For scramjets, previous studies mainly consider the full engine size (global scale) as a flow characteristic length, and the incoming velocity[12] or the mid-axis flow velocity[13] as the characteristic speed. However, this global view hardly helps to know the local state of thermochemical nonequilibrium all over the high-Mach scramjet. Compared to engines operating at flight Mach numbers of 4–7, where the flow residence time is relatively longer and global scale calculations can reasonably approximate the flow behavior, engines operating at flight Mach numbers over 8 face significantly shortened residence time in the scramjet. The reduction of flow residence time significantly increases the challenge of judging thermochemical nonequilibrium state at local regions. Therefore, the local length scale needs to be sought for calculating the local flow residence time as required.

For the chemical reaction timescale, there are different definitions for different chemical/combustion reaction systems in previous studies, mainly categorized into the eigenvalue based and algebraic expressions.[14] The eigenvalue based methods use the inverse eigenvalues of

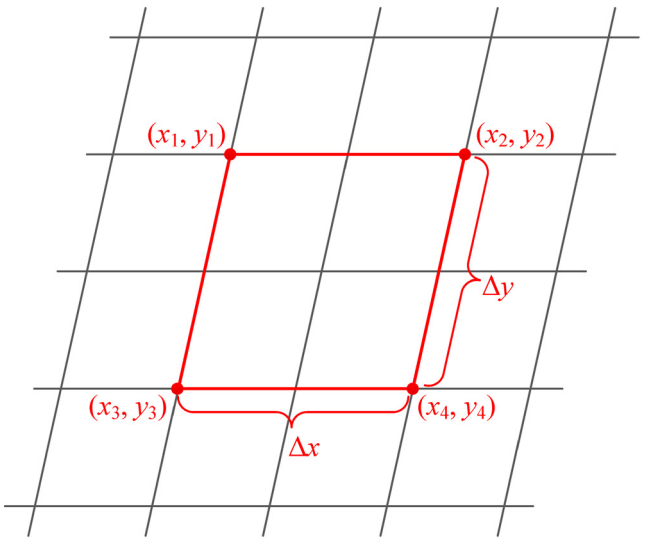

FIG. 1. Sketch of local length across a two-grid scale for flow residence time calculation.

chemical reaction system as the chemical reaction timescales by calculating or approximating the Jacobian matrix of chemical reaction source term and its decomposition. In contrast, the algebraic methods calculate timescales using a combination of species concentrations, chemical reaction rates, and/or species consumption rates, with more simplicity and higher computational efficiency. There are two commonly used algebraic approaches formulating chemical reaction timescales. One is based on the change rate of species, equivalent to the timescale of species production/destruction. For example, Evans *et al.*[15] calculated the chemical timescales using the change rates of species to evaluate *Da* in turbulent combustion flow simulation. The other is based on the chemical reaction rate, actually how fast the chemical reaction proceeds. For this method, the simplest way is using the reciprocal of reaction rate coefficient ($1/k_r$) as the chemical timescale.[14] As mentioned earlier, one problem naturally arises: different definitions of chemical timescales might deduce different characteristics of thermochemical nonequilibrium in the scramjet.

To show a clear map of thermochemical nonequilibrium in the whole scramjet, the present study first develops a scheme to calculate the local flow residence time based on the computational fluid dynamics (CFD) mesh and proposes the methods to compute the timescales of thermodynamically vibrational relaxation and chemical reaction, which are used for determining Damköhler number to judge the nonequilibrium state. Then, two cases of thermochemical nonequilibrium combustion flows in Deutsches Zentrum für Luft-und Raumfahrt (DLR)[16] and HyShot II[17] scramjets are simulated, respectively, to evaluate the thermochemical nonequilibrium features in the scramjets. The in-house CFD solver PHAROS, which has been fully validated with high reliability and fidelity in many previous studies,[18–21] is used for the simulations. Finally, the comprehensive regionalization of thermochemical nonequilibrium in both scramjets is shown and discussed at different observational length scales.

The compressible turbulent combustion flow in the scramjet is computed using the Favrè-averaged Navier–Stokes equations, as outlined in Eqs. (1)–(4) in the research by Gao *et al.*,[22] and Menter's k-ω SST two-equation model for turbulence closure, as given in Eqs. (5) and (6) from Menter *et al.*[23] The thermodynamically vibrational nonequilibrium is characterized by the Park two-temperature model, where the combined energy of translational and rotational modes is described by one translational temperature, while the combined energy of electron, electronic energy, and vibrational modes is represented by one vibrational temperature.[24,25] The hydrogen (H_2)–air chemical reaction kinetic model, which contains seven species and eight reactions proposed by Spiegler *et al.*, is used.[26]

In this study, the degrees of thermodynamically vibrational and chemical nonequilibrium are evaluated using the vibrational Damköhler number $Da_V = \tau_f/\tau_V$ and the chemical Damköhler number $Da_{chem} = \tau_f/\tau_{chem}$, respectively, where τ_f, τ_V, and τ_{chem} are the timescales of flow residence, thermodynamically vibrational relaxation, and chemical/combustion reaction.

The flow residence time is significantly related to the spatial length scale that the flow passes through. Therefore, the present study proposes a computational method of flow residence time related to observational length scale based on the CFD mesh. The local flow residence time, $\tau_{f,\,local}$, and the global flow residence time, $\tau_{f,\,global}$, are defined, respectively, as follows:

$$\tau_{f,local} = \min\left\{\frac{\Delta x}{u}, \frac{\Delta y}{v}\right\}, \tag{1}$$

$$\tau_{f,global} = \frac{L}{u_\infty}, \tag{2}$$

$$\Delta x = \max\{x_1, x_2, x_3, x_4\} - \min\{x_1, x_2, x_3, x_4\}, \tag{3}$$

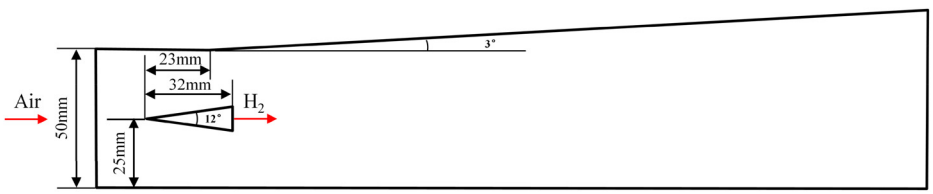

FIG. 2. Schematic of the DLR combustor.

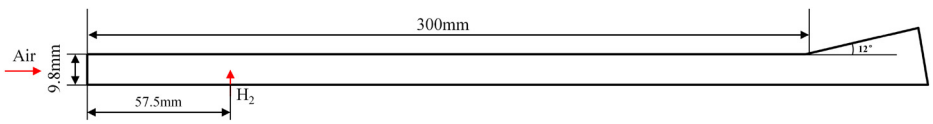

FIG. 3. Schematic of the HyShot II combustor.

TABLE I. DLR air inflow and hydrogen jet conditions.

	Ma	T_∞ (K)	P_∞ (kPa)	Y_{H2}	Y_{O2}	Y_{H2O}	Y_{N2}
Air	2.0	340	100	0.0	0.232	0.032	0.736
H_2	1.0	250	100	1.0	0.0	0.0	0.0

TABLE II. HyShot II air inflow and hydrogen jet conditions.

	Ma	T_∞ (K)	P_∞ (kPa)	Y_{H2}	Y_{O2}	Y_{H2O}	Y_{N2}
Air	2.49	1370	127	0.0	0.235	0.0	0.765
H_2	1	300	315	1.0	0.0	0.0	0.0

$$\Delta y = \max\{y_1, y_2, y_3, y_4\} - \min\{y_1, y_2, y_3, y_4\}, \quad (4)$$

where Δx and Δy denote the local lengths across a certain number of CFD grids in the x- and y-directions, respectively, as shown in Fig. 1; u and v represent the local velocity component in the x- and y-directions, and u_∞ is the incoming flow velocity.

TABLE III. Size of each observational length scale.

Observational length scale	Length size (unit: m)	
	DLR	HyShot II
2-grid scale	2×10^{-4}–6×10^{-3}	2×10^{-6}–1×10^{-3}
20-grid scale	1×10^{-3}–5×10^{-2}	3×10^{-5}–1×10^{-2}
Global scale	0.3	0.35

The thermodynamically vibrational relaxation time of the species s collision with the species m, $\tau_{V,\,s\text{-}m}$, is calculated by the Millikan–White relation as follows:

$$\tau_{V,s-m} = \frac{1}{p}\exp\left[0.00116\mu_{sm}^{1/2}\theta_{vs}^{4/3}(T^{-1/3} - 0.015\mu_{sm}^{1/4}) - 18.42\right], \quad (5)$$

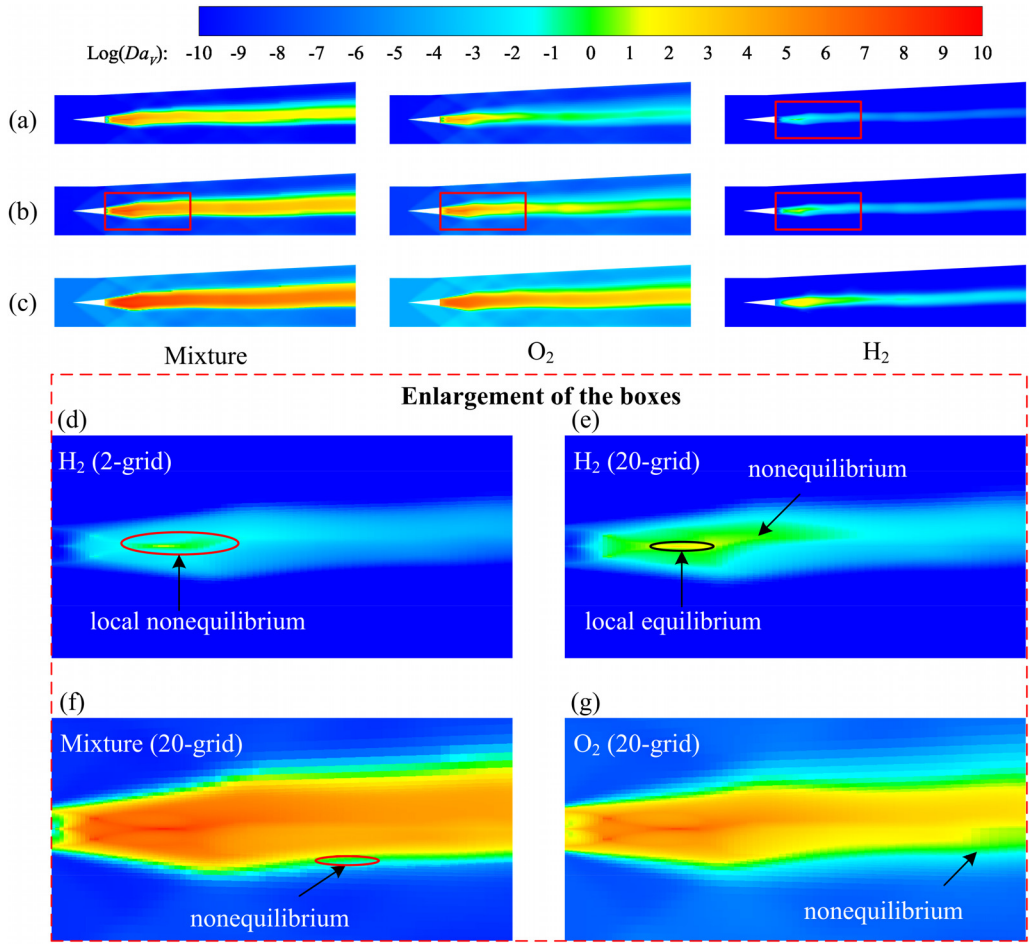

FIG. 4. Da_V in the DLR scramjet at different observational scales: (a) 2-grid scale; (b) 20-grid scale; (c) global scale. (d)–(g) Enlarged views of the boxed regions.

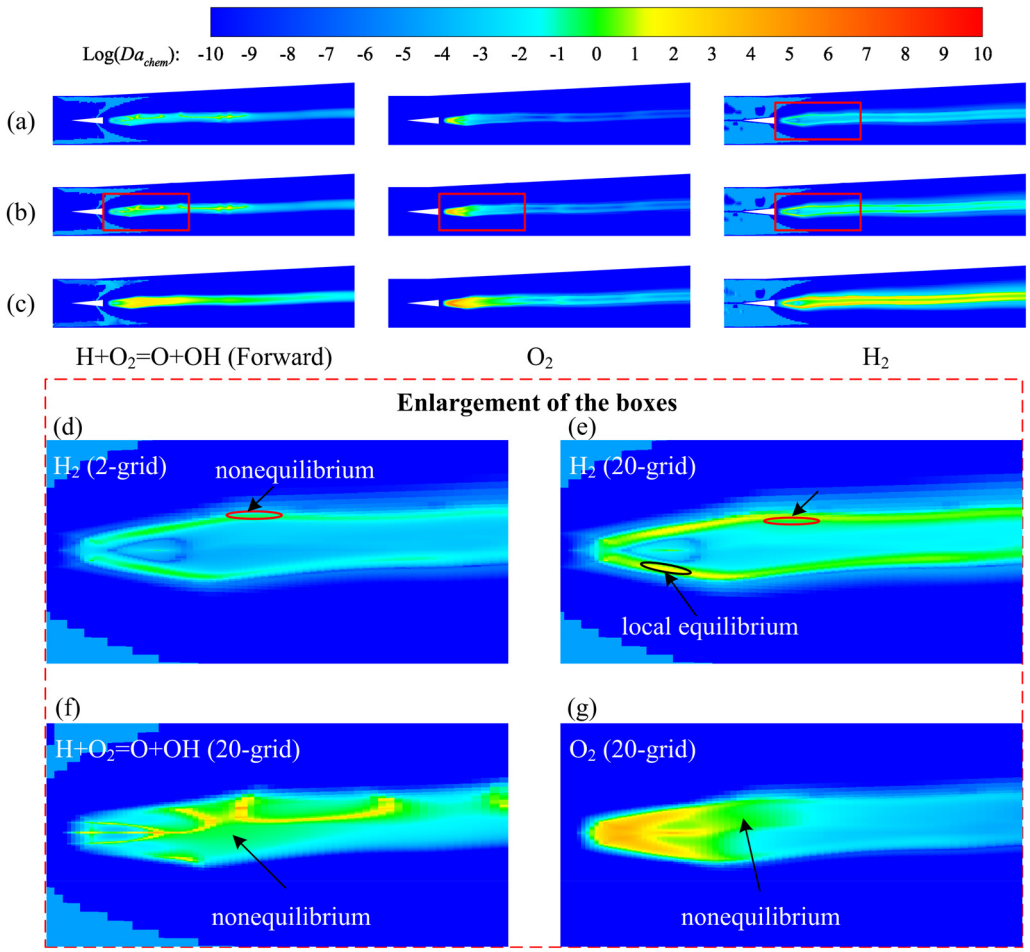

FIG. 5. Da_{chem} in the DLR scramjet at different observational scales: (a) 2-grid scale; (b) 20-grid scale; (c) global scale. (d)–(g) Enlarged views of the boxed regions.

$$\tau_{V,s} = \frac{\sum_m X_m}{\sum_m X_m/\tau_{V,s-m}}, \tag{6}$$

where p is the static pressure in atm, T is the translational temperature, μ_{sm} denotes the reduced molecular weight of the species s and m, θ_{vs} is the characteristic vibrational temperature of the species s, $\tau_{V,s}$ is the thermodynamically vibrational relaxation time of the species s, and X_m is the molar fraction of the species m. The total thermodynamically vibrational relaxation time of gas mixture, τ_V, is calculated using the expression proposed by Ao *et al.*[24] as follows:

$$\tau_V = \frac{\sum_{s=mol.} X_s}{\sum_{s=mol.} X_s/\tau_{V,s}}, \tag{7}$$

where the subscript "*mol.*" represents the molecular species.

Two commonly used algebraic methods for calculating the chemical reaction timescales are both employed in the present study. The chemical reaction timescale, $\tau_{chem,\,s}$, based on the change rate of species s, ω_s, is proposed by Wartha *et al.*[14] as follows:

$$\tau_{chem,s} = \frac{\rho_s}{\omega_s}, \tag{8}$$

where ρ_s is the density of species s.

The chemical reaction timescale, $\tau_{chem,\,r}$, based on the rth chemical reaction rate, R_r, is formulated as follows:

$$\tau_{chem,r} = \frac{\rho}{M}\cdot\frac{1}{R_r}, \tag{9}$$

where ρ and M denote the total density and mean molecular weight of the gas mixture.

The two-dimensional sketches of DLR and HyShot II scramjets refer to Oevermann[16] and Laurence *et al.*,[17] as shown in Figs. 2 and 3, respectively. The air inflow and hydrogen jet conditions are listed in Tables I and II, respectively. For the wall boundary conditions, an isothermal wall is set, with both upper and lower wall temperatures fixed at 300 K. To guarantee the prediction precision, the dimensionless distance of the first layer grid near the wall for both cases, y^+, is close to

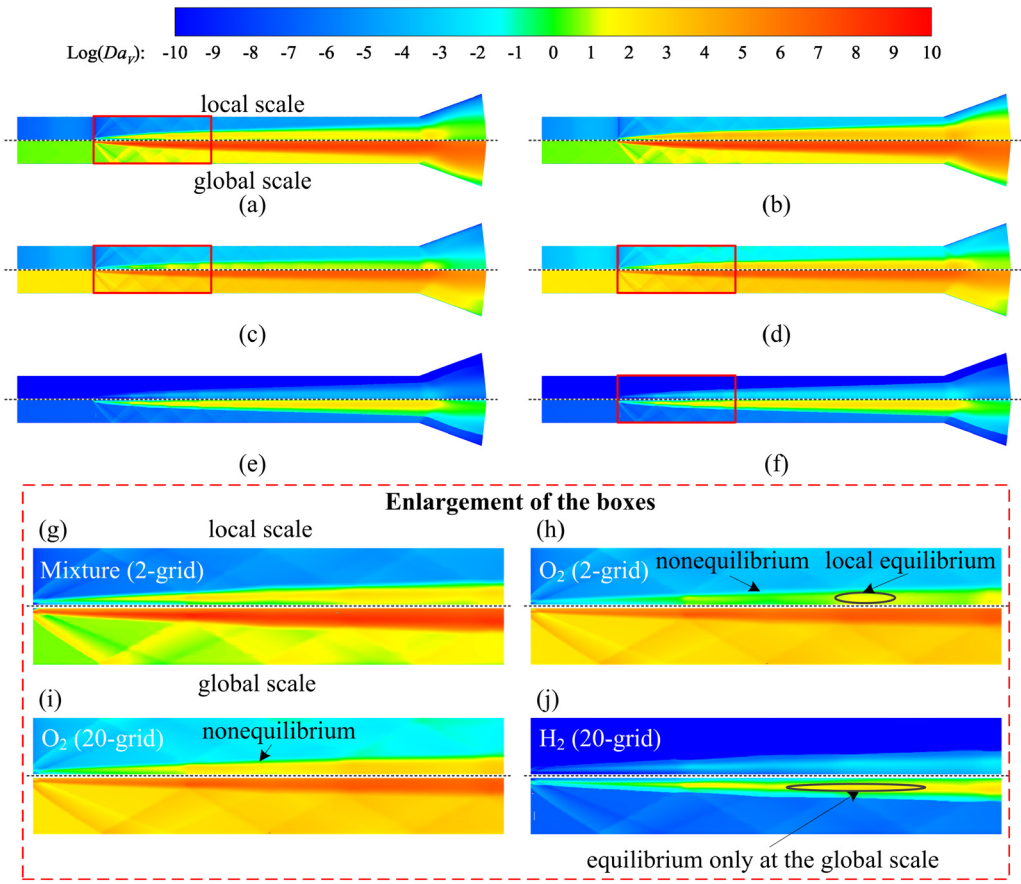

FIG. 6. Da_V in the HyShot II scramjet at the local scale (top) and global scale (bottom), taking the gas mixture (a) and (b), species O_2 (c) and (d), and species H_2 (e) and (f) as examples. Local scale results are shown for the 2-grid scale (a), (c), (e) and 20-grid scale (b), (d), (f), respectively. (g)–(j) Enlarged views of the boxed regions.

1.0.[27] The flow field is initialized using the air inflow parameters in Tables I and II. The simulations are performed in a two-dimensional configuration.

The thermodynamically vibrational relaxation times are calculated for each molecular species (H_2, N_2, O_2, OH, H_2O) and gas mixture. The chemical reaction times for seven species (H, O, H_2, N_2, O_2, OH, H_2O) and for 16 chemical reactions (eight forward and eight backward reactions) are all calculated. Flow residence times are calculated using two local length scales, across 2 and 20 grids and a full engine size, respectively. The size of each observational length scale for flow residence time calculation, based on the same set of grids, is listed in Table III. The values of vibrational Damköhler number, Da_V, and chemical Damköhler number, Da_{chem}, distributed in DLR and HyShot II scramjets, are both computed based on CFD results. Vibrational or chemical nonequilibrium is recognized as Da_V or Da_{chem} in the range of 0.1–10, while flows are recognized as frozen (Da_V or Da_{chem} less than 0.1) or in equilibrium (Da_V or Da_{chem} more than 10) outside this range. To avoid abnormally too large or too small Da values, the flow is set to be thermochemically frozen when the mass fraction of species is less than 10^{-6}.

The thermochemical maps of DLR and HyShot II scramjets based on different observational length scales are shown in Figs. 4–7, respectively. The thermodynamically vibrational nonequilibrium cases take the gas mixture, the species O_2 and H_2 as examples, while the chemical nonequilibrium cases take the forward reaction of $H + O_2 = O + OH$, with species O_2 and H_2 as examples. According to Eq. (1), the flow residence time τ_f strongly depends on the observational length scale. Figures 4–7 show that as the length scale for τ_f extends, both vibrational Damköhler number Da_V and chemical Damköhler number Da_{chem} rise, and the thermochemical nonequilibrium zone remarkably spreads in DLR and HyShot II scramjets.

In Figs. 4 and 5, the inflow of the DLR scramjet is thermochemically frozen at all three observational scales. To show critical details, localized magnifications of some key regions are provided in Figs. 4 and 5. In the DLR scramjet, the vibrational nonequilibrium mainly locates at the edge of the flame, while the chemical nonequilibrium is primarily located inside the combustion flame. Both Da_V and Da_{chem} have the highest level in the flame region with high temperature, where the gas mixture and O_2 are in vibrational equilibrium at all scales, but H_2 begins to show the obvious local vibrational equilibrium at the length scale across 20 grids, as shown in Figs. 4(d) and 4(e). Therefore, the thermochemical characteristics at the local scale are not very consistent with those at the global scale.

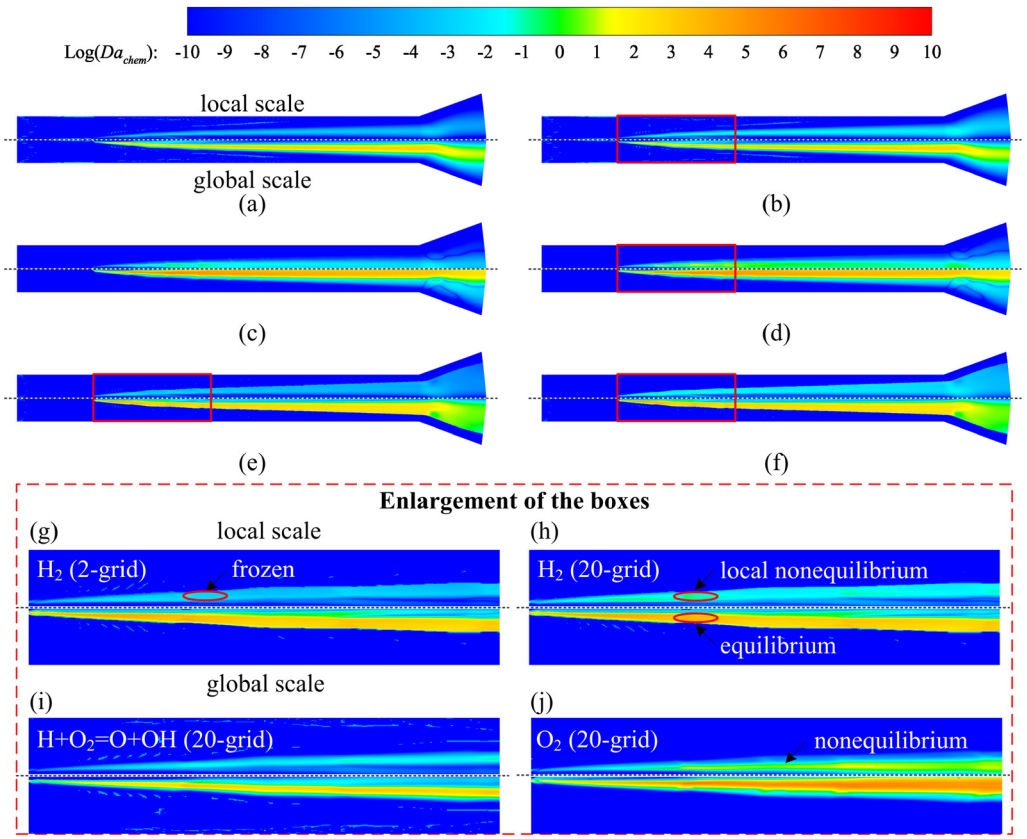

FIG. 7. Da_{chem} in the HyShot II scramjet at the local scale (top) and global scale (bottom), taking the forward reaction of $H + O_2 = O + OH$ (a) and (b), species O_2 (c) and (d), and species H_2 (e) and (f) as examples. Local scale results are shown for the 2-grid scale (a), (c), (e) and 20-grid scale (b), (d), (f), respectively. (g)–(j) Enlarged views of the boxed regions.

As shown in Fig. 6, the inflow in front of the H_2 jet in the HyShot II scramjet is vibrationally frozen for two grid scales. However, at the global scale, the inflow thermodynamic states of different species are not consistent, where the gas mixture is in vibrational nonequilibrium, O_2 is in vibrational equilibrium, and H_2 is vibrationally frozen. Figure 6 also provides enlarged views of key regions. In the flame region with the highest level of Da_V, the gas mixture and O_2 achieve the vibrational equilibrium at all scales, while H_2 is remarkably in vibrational equilibrium only at the global scale, as clearly shown in Fig. 6(j). The vibrational nonequilibrium in the HyShot II scramjet is still basically located at the edge of the flame. As the observational scale rises, the vibrational equilibrium region becomes wider in the scramjet, as exemplified by the Da_V distribution of O_2 at all three observational scales in Figs. 6(h) and 6(i).

In Fig. 7, the inflow of the HyShot II scramjet is chemically frozen at all scales. Figures 7(g)–7(j) show magnified details of critical regions. Da_{chem} based on O_2 and H_2 exhibits a wider distribution of chemical nonequilibrium compared to that based on the forward reaction of $H + O_2 = O + OH$, which is clearly shown in Figs. 7(h)–7(j). For both kinds of Da_{chem}, the chemical nonequilibrium is mainly inside the high-temperature flame zone. As the observational scale increases, the flow states in some parts of the scramjet change from the chemically frozen to the chemically nonequilibrium and even equilibrium, such as Da_{chem} distribution of H_2 at all three observational scales in Figs. 7(g) and 7(h).

To calculate the vibrational and chemical Damköhler numbers, a method based on CFD mesh is developed to obtain the local flow residence time. The vibrational relaxation timescale is calculated using the Millikan–White relation, and the chemical timescale is computed using both the species based and reaction based methods. Two cases of thermochemical nonequilibrium combustion flows in DLR and HyShot II scramjets are simulated to show the detailed zonal characteristics of thermochemical nonequilibrium based on Da_V and Da_{chem} distributions at different observational length scales, which has not been shown in previous studies. The main conclusions are as follows:

(1) The observational length scale has a crucial impact on the flow residence time and Damköhler number calculations, thereby significantly affecting the thermochemical nonequilibrium characteristics in the scramjet.
(2) The thermochemical maps of DLR and HyShot II scramjets shows that, as the observational length scale extends, both vibrational and chemical Damköhler number rise, and the thermochemical nonequilibrium zone remarkably spreads.

(3) Generally, the vibrational nonequilibrium is mainly located at the edge of the flame, while the chemical nonequilibrium is primarily located inside the combustion flame.

In a word, existing studies of thermochemical nonequilibrium in scramjets at the global scale are insufficient, and those at the local scale should also be paid attention to in future research.

ACKNOWLEDGMENTS

This work was supported by the National Natural Science Foundation of China (Grant No. 12002193); the Shandong Provincial Natural Science Foundation, China (Grant No. ZR2019QA018); and the "Xin Feng Xiang" Project of Key Laboratory of Hypersonic Aerodynamic Force and Heat Technology, AVIC Aerodynamics Research Institute (Grant No. XFX20220102).

AUTHOR DECLARATIONS

Conflict of Interest

The authors have no conflicts to disclose.

Author Contributions

Jingying Wang: Conceptualization (equal); Data curation (lead); Formal analysis (equal); Funding acquisition (lead); Investigation (lead); Methodology (equal); Project administration (lead); Validation (equal); Visualization (lead); Writing – original draft (equal); Writing – review & editing (equal). **Shiyue Zhang:** Formal analysis (equal); Methodology (equal); Resources (equal); Validation (equal); Writing – original draft (equal). **Jiaao Hao:** Resources (equal); Software (equal); Supervision (lead); Writing – original draft (equal). **Wei Zhao:** Resources (equal); Validation (equal). **Xinglian Yang:** Visualization (equal). **Chunhian Lee:** Supervision (supporting).

DATA AVAILABILITY

The data that support the findings of this study are available from the corresponding author upon reasonable request.

REFERENCES

[1]J. Zhang, Z. Wang, C. Liu, M. Sun, H. Wang, J. Ai, and Z. Zhang, "Thermochemical nonequilibrium effects on combustion characteristics of a transverse jet in the scramjet," Aerosp. Sci. Technol. **152**, 109357 (2024).
[2]P. P. Nair, J. Ananthu, and V. Narayanan, "Effect of jet splitting using passive strut on the performance and thermoacoustic characteristics of a scramjet combustor," Phys. Fluids **36**, 086114 (2024).
[3]W. Yao, "Nonequilibrium effects in hypersonic combustion modeling," J. Propul. Power **38**, 523 (2022).
[4]W. Yao, H. Liu, Z. Zhang, X. Zhang, L. Yue, X. Zhang, and J. Li, "Effects of thermal/chemical nonequilibrium on a high-Mach ethylene-fueled scramjet," J. Propul. Power **39**, 562 (2023).
[5]R. Fiévet and V. Raman, "Effect of vibrational nonequilibrium on isolator shock structure," J. Propul. Power **34**, 1334 (2018).
[6]H. Koo, V. Raman, and P. L. Varghese, "Direct numerical simulation of supersonic combustion with thermal nonequilibrium," Proc. Combust. Inst. **35**, 2145 (2015).
[7]R. Fiévet, S. Voelkel, H. Koo, V. Raman, and P. L. Varghese, "Effect of thermal nonequilibrium on ignition in scramjet combustors," Proc. Combust. Inst. **36**, 2901 (2017).
[8]H. Liu, W. Yao, X. Zhang, X. Zhang, J. Liu, L. Yue, and Q. Sun, "Nonequilibrium heating/cooling effects in a Mach number 10 hydrogen-fueled scramjet," J. Propul. Power **40**, 337 (2024).
[9]X. Li, Z. Wang, J. Cao, T. Shen, and J. Du, "Numerical study on auto-ignition and combustion characteristics in a supersonic combustor without flame-holder," Aerosp. Sci. Technol. **144**, 108792 (2024).
[10]K. Neitzel, D. Andrienko, and I. D. Boyd, "Aerothermochemical nonequilibrium modeling for oxygen flows," J. Thermophys. Heat Trans. **31**, 634 (2017).
[11]S. Srivastava and S. S. Sinha, "Influence of vibrational and chemical nonequilibrium on the velocity-gradient and the pressure-Hessian fields in compressible turbulence," Phys. Fluids **37**, 015144 (2025).
[12]J. Zuo, J. Xue, S. Zhang, J. Wei, X. Li, N. Cui, and W. Bao, "Combustion performance of hydrogen fueled parallel wall-jet used for drag reduction in a supersonic combustor," Case Stud. Therm. Eng. **59**, 104490 (2024).
[13]G. N. Jovanovic, M. Y. Coblyn, and I. Plazl, "Time scale analysis & characteristic times in microscale-based chemical and biochemical processes: Part I-Concepts and origins," Chem. Eng. Sci. **238**, 116502 (2021).
[14]E. M. Wartha, M. Bösenhofer, and M. Harasek, "Characteristic chemical time scales for reactive flow modeling," Combust. Sci. Technol. **193**, 2807 (2021).
[15]M. Evans, C. Petre, P. R. Medwell, and A. Parente, "Generalisation of the eddy-dissipation concept for jet flames with low turbulence and low Damköhler number," Proc. Combust. Inst. **37**, 4497 (2019).
[16]M. Oevermann, "Numerical investigation of turbulent hydrogen combustion in a SCRAMJET using flamelet modeling," Aerosp. Sci. Technol. **4**, 463 (2000).
[17]S. Laurence, S. Karl, J. M. Schramm, and K. Hannemann, "Transient fluid-combustion phenomena in a model scramjet," J. Fluid Mech. **722**, 85 (2013).
[18]J. Wang, J. Hao, and G. Du, "Numerical analysis of the aerodynamic heating in hypersonic thermo-chemical nonequilibrium flows," in 21st AIAA International Space Planes and Hypersonics Technologies Conference (2017).
[19]J. Wang, F. Han, L. Lei, and C. Lee, "Numerical study of high-temperature non-equilibrium flow around reentry vehicle coupled with thermal radiation," Fluid Dyn. Mater. Process **16**, 601 (2020).
[20]Z. Gao, J. Wang, C. Jiang, and C. Lee, "Application and theoretical analysis of the flamelet model for supersonic turbulent combustion flows in the scramjet engine," Combust. Theory Model. **18**, 652 (2014).
[21]J. Hao, J. Wang, and C. Lee, "Assessment of vibration-dissociation coupling models for hypersonic nonequilibrium simulations," Aerosp. Sci. Technol. **67**, 433 (2017).
[22]Z. Gao, C. Jiang, S. Pan, and C. Lee, "Combustion heat-release effects on supersonic compressible turbulent boundary layers," AIAA J. **53**, 1949 (2015).
[23]F. R. Menter, "Two-equation eddy-viscosity turbulence models for engineering applications," AIAA J. **32**, 1598 (1994).
[24]Y. Ao, K. Wu, H. Lu, F. Ji, and X. Fan, "Combustion dynamics of high Mach number scramjet under different inflow thermal nonequilibrium conditions," Acta Astronaut. **208**, 281 (2023).
[25]C. Park, "The limits of two-temperature model," AIAA Paper No. 2010-911 (2010).
[26]E. Spiegler, M. Wolfshtein, and Y. Manheimer-Timnat, "A model of unmixedness for turbulent reacting flows," Acta Astronaut. **3**, 265 (1976).
[27]A. Joshi, A. Assam, M. Nived, and V. Eswaran, "A generalised wall function including compressibility and pressure-gradient terms for the Spalart-Allmaras turbulence model," J. Turbul. **20**, 626 (2019).